Generalised Analysis of Compensating Balancing Sleeves with Experimental Results from a Scaled Industrial Turbine Coupling Shaft

Journal:	*Part C: Journal of Mechanical Engineering Science*
Manuscript ID	JMES-17-0241.R1
Manuscript Type:	Original article
Date Submitted by the Author:	10-Jul-2017
Complete List of Authors:	Knowles, James; University of Lincoln, School of Engineering Kirk, Antony; University of Lincoln, School of Engineering Bingham, Chris; University of Lincoln Bickerton, Ron; University of Lincoln, School of Engineering
Keywords:	High-Speed Shafts, Lateral Vibrations, Balancing Sleeve, Critical Speed, Mechanical Design
Abstract:	The paper furthers the analysis of a recently proposed balancing methodology for high-speed, flexible shafts. This mechanism imparts corrective balancing moments, having the effect of simulating the fixing moments of equivalent double or single encastre mounted shafts. This is shown to theoretically eliminate/nullify the 1st lateral critical speed (LCS), and thereby facilitate safe operation with reduced LCS margins. The paper extends previously reported research to encompass a more generalised case of multiple, concentrated, residual imbalances, thereby facilitating analysis of any imbalance distribution along the shaft. Solutions provide greater insight of the behaviour of the balancing sleeve concept, and the beneficial implications for engineering design. Specifically: 1) a series of concentrated imbalances can be regarded as an equivalent level of uniform eccentricity, and balance sleeve compensation is equally applicable to a generalised unbalanced distribution, 2) compensation depends on the sum of the applied balancing sleeve moments and can therefore be achieved using a single balancing sleeve (thereby simulating a single encastre shaft), 3) compensation of the 2nd critical speed, and to a lesser extent higher orders, is possible by use of two balancing sleeves, positioned at shaft ends, 4) the concept facilitates on-site commissioning of trim balance which requires a means of adjustment at only one end of the shaft, 5) the Reaction Ratio, RR, (simply supported/ encastre), is independent of residual eccentricity, so that the implied benefits resulting from the ratio (possible reductions in the equivalent level of eccentricity) are additional to any balancing procedures undertaken prior to encastre simulation. Analysis shows that equivalent reductions in the order of 1/25th, are possible. Experimental measurements from a scaled model of a typical drive coupling employed on an industrial gas turbine package, loaded asymmetrically with a concentrated point of imbalance, are used to support the analysis and conclusions.

Original article

Generalised Analysis of Compensating Balancing Sleeves with Experimental Results from a Scaled Industrial Turbine Coupling Shaft

Grahame Knowles

(School of Engineering) University of Lincoln, UK

Antony Kirk

(School of Engineering) University of Lincoln, UK

Chris Bingham

(School of Engineering) University of Lincoln, UK

Ron Bickerton

(School of Engineering) University of Lincoln, UK

Corresponding Author:

Grahame Knowles, School of Engineering, University of Lincoln, Brayford Pool,

Lincoln, LN6 7TS, UK.

Email: grahameknowles@yahoo.ac.uk

Abstract

The paper furthers the analysis of a recently proposed balancing methodology for high-speed, flexible shafts. This mechanism imparts corrective balancing moments, having the effect of simulating the fixing moments of equivalent double or single encastre mounted shafts. This is shown to theoretically eliminate/nullify the 1st lateral critical speed (LCS), and thereby facilitate safe operation with reduced LCS margins. The paper extends previously reported research to encompass a more generalised case of multiple, concentrated, residual imbalances, thereby facilitating analysis of any imbalance distribution along the shaft. Solutions provide greater insight of the behaviour of the balancing sleeve concept, and the beneficial implications for engineering design. Specifically: 1) a series of concentrated imbalances can be regarded as an equivalent level of uniform eccentricity, and balance sleeve compensation is equally applicable to a generalised unbalanced distribution, 2) compensation depends on the sum of the applied balancing sleeve moments and can therefore be achieved using a single balancing sleeve (thereby simulating a single encastre shaft), 3) compensation of the 2nd critical speed, and to a lesser extent higher orders, is possible by use of two balancing sleeves, positioned at shaft ends, 4) the concept facilitates on-site commissioning of trim balance which requires a means of adjustment at only one end of the shaft, 5) the Reaction Ratio, *RR*, (simply supported/ encastre), is independent of residual eccentricity, so that the implied benefits resulting from the ratio (possible reductions in the equivalent level of eccentricity) are additional to any balancing procedures undertaken prior to encastre simulation. Analysis shows that equivalent reductions in the order of 1/25th, are possible. Experimental measurements from a scaled model of a typical drive coupling employed on an industrial gas turbine package, loaded asymmetrically with a concentrated point of imbalance, are used to support the analysis and conclusions.

Keywords: High-speed shafts, lateral vibrations, balancing sleeve, critical speed, mechanical design

1. Introduction

All shafts and rotors contain a degree of mass unbalance due to asymmetry and manufacturing imperfection leading to forces being exerted by the rotor on its surrounding structures. It is of considerable importance to ensure that such forces are appropriately accommodated either by design or by addressing the geometric unbalance of the rotor[1]. Attempts to achieve this through design and precise tolerancing during rotor manufacture are frequently insufficient, and alternative means of reducing vibration levels are therefore necessary, typically employing post-manufacture dynamic balancing.

The impact of such problems can be identified in diverse application fields, ranging from the use of high speed dentist drills, to gas turbines for the oil and gas industry, where couplings between prime movers (eg. gas turbine) and driven units (e.g. compressors) have tended to become longer and operate at higher speeds as designs have advanced[2]. Safe operation is ensured by adherence to American Petroleum Institute (API) design rules, which have increasingly strict requirements to limit both torsional and lateral vibration. For some installations these limits can often be difficult to achieve. For instance, in the case of flexible coupling shafts the lateral critical speed margin is now 1.5 or 2 times the maximum operating speed[3]. As a consequence there is significant interest in lateral critical speed margins[4], as they often result in additional costs and design limitations as they become higher. For a given length, coupling design (for gas turbines in the oil and gas industry, for example) is often a compromise between the coupling lateral flexibility (i.e. maintaining a suitable lateral critical speed margin), its maximum diameter (in order to limit the effects of churning), and the need to meet ½ mass requirements of the driven unit[5]. A consequence is that from a balancing perspective, couplings are often more flexible than desirable and are extremely difficult to dynamically balance across a wide operating speed range.

For a rigid rotor with two unbalanced forces acting in two planes, the induced vibration is a transverse bounce or tilting motion without any flexing of the rotor. This dynamic unbalance is corrected by two balance weights being radially positioned in the two different planes, either in-phase or 180 degrees out of phase, as necessary. If a rigid rotor is balanced using two planes at any speed, it is considered balanced at all speeds. However, this is not the case for a flexible rotor, particularly when operating at high-speeds.

Modal balancing[6], consists of the addition of small masses at the surface of the rotor in a manner that cancels the effects of eccentricity. At low speeds, i.e. those well below the first critical

frequency, a flexible rotor can be assumed as a rigid body and there is no deflection due to eccentricity. Despite this, there may be a considerable increase in centrifugal forces that are transferred to the bearings. The purpose of low speed balancing is to ensure that the axis of rotation is a principal axis of inertia in order to nullify the moments of the inertia forces. At high speeds close to or beyond the first critical frequency, balancing as a rigid rotor becomes detrimental since the addition of balance weights can cause large deflections across a range of speeds. Moreover, due of the widespread use of low-speed balancing machines and the difficulties in approximating the balance correction required for high-speed use, a number of alternative balancing methodologies have been proposed based on the assumed modal shape of the shaft[7], or else underpinned by significant a-priori knowledge of the unbalance characteristics[8]. However, due to (typically) unknown imbalance distributions, balancing errors caused by shaft deflection are not adequately catered for across the required operating speed range and many field problems persist where unacceptably high vibrations at the bearings lead to subsequent unit shutdowns and failures.

In recognition that low speed balancing is often inadequate for application to flexible rotors (particularly those that operate close to, or must pass through, critical speeds), other more general methodologies to balance shafts have been investigated. Typically, for each critical speed that a rotor must traverse, a different state of balance is required, and therefore different balance planes are necessary. The axial location where balance masses have most effect in mitigating vibrations excited at a critical speed can be identified either numerically, analytically or empirically, but in each case to achieve modal balance some knowledge of the rotor's dynamic behaviour is necessary. In the latter case, when balancing a particular mode, a trial mass is added to a series of locations and the amplitude of the resulting vibration is measured close to the associated critical speed until the minimum vibration amplitude is identified. This method is known to achieve precise levels of balance, but is considered very time-consuming.

Alternative methods for conducting modal balancing without the use of trial masses attempt to model a rotor system based on measured characteristics[9]. This approach typically requires assumptions to be made regarding the bearings, which are difficult to model accurately or else require running vibration measurements to be taken. A further alternative method, termed influence coefficient balancing[10], selects correction masses to be placed in positions to ensure that vibration is zero at a series of known locations along the shaft for a series of shaft speeds. Although successful, this technique requires substantial theoretical and computational analysis.

More recent work has concentrated on the possibility of 'automatic balancing' whereby masses have limited movement to allow for balancing across a range of speeds. Reported research[11], for instance, was limited to a rigid rotor where the degree and position unbalance may change over time, and it remains difficult to achieve satisfactory results consistently over a large speed range for flexible shafts or rotors. Meanwhile, the use of controllable bearings, actuators and sensors to measure and control vibration continues to be work-in-progress research, due to the complexities surrounding the control system and the likely high-cost of implementation, as report[12] and more recent report[13] which made a detailed study of the vibration control characteristics of gas foil bearings with inbuilt electromagnetic actuators.

As an alternative to the above approaches, a novel method of balancing long, flexible, high-speed drive shafts has been proposed[14,15], where balance corrections (that are traditionally applied to the ends of the drive shaft) are applied instead to the free ends of a pair of balancing sleeve arms, integrally attached to each end of the drive shaft. The balance sleeve applies a corrective centrifugal force to the drive shaft to limit the shaft-end reaction forces. As well as increasing with speed, the correcting forces also increase in magnitude due to the flexibility of the balancing sleeve. This mechanism of attaching trim balance masses therefore counteracts the increased shaft imbalance forces resulting from the shaft's own flexibility, and provides a means of amplifying the balance correction set at low-speed to reduce the balancing errors produced at high speed by shaft deflection. Additionally, it also imparts a corrective bending moment to the drive shaft that has a beneficial tendency to limit the shaft deflection and may be set by replicating the fixing moments of an encastre mounted shaft to theoretically nullify (i.e. move to a higher speed) the original critical speed of a simply supported shaft. Various detailed forms are possible such as light weight, low profile designs - to minimise windage losses, for external application - with fixed or adjustable length, moment arms and suitable for either original equipment, (OE), or retro fitting. Alternatively, designs can be tailored to suit internal deployment within hollow sections of shafts, with external, manual or remotely/electrically actuated adjustment.

It is shown here that this mechanism is beneficial on shaft systems with high flexibility and/or high shaft deflection, but is most likely to occur in practice when the shaft is mounted in angularly, non-restraining bearings, e.g. rolling element ball, or short, high clearance journal bearings. The latter is commonly used in industrial prime mover and driven units such as those used in the Oil and Gas Market, where design standards, ISO 7919-4[16]; ISO 10816-4[17] typically

require vibration monitoring/ proximity sensors and software to shut down units if shaft movements exceed a percentage of the bearing clearance, (eg. 60%), in order to prevent bearing 'wipe-out'. The method is also applicable when long, flexible-element, coupling-shafts are employed — the latter being regarded as having 'moment release', i.e. the elements act as a lateral hinge. Hence, such shafts can be modelled as being simply supported and are more flexible as a consequence, making them particularly suitable to this method of balancing. Previously reported research on balancing sleeves[12] has only considered the specialised case of plain shafts with uniform eccentricity. Here, the presented treatment now develops a generalised extended approach that is applicable to more realistic imbalance distributions, comprising multiple concentrations of imbalance of variable magnitude, revealing several new insights with practical benefits for engineering design.

2. Theoretical Analysis

Following previously reported studies[14] a simply supported, long, plain shaft, of circular cross section (making gyroscopic moments negligible) operating under steady state rotating conditions, and where both radial and angular accelerations and associated forces/ moments are zero, is considered. This provides a first-order simplification that is widely considered applicable to long, thin shafts, with low slenderness ratios[18], typically < 0.12 (as employed in the site-equivalent case study models given later). Shaft deflections due to shear effects are regarded as "second degree" in magnitude, and are therefore not considered further. For derivation simplicity, the initial study is limited to a single concentrated imbalance, as it is further shown that more complex distributions can be regarded as the summation of any number of individual imbalances, provided that the shaft deflections remain small and the material is operating within the linear portion of its stress/ strain curve (the principle of superposition then becomes applicable). This approach allows algebraic solutions to be obtained from the equations of motion, negating the requirement for time-consuming numeric solutions from Finite Element Analysis (FEA) to be necessary during early design stages.

Figure 1 shows a plain rotating shaft of total mass, M_s, and overall length, ℓ, simply supported at both ends, with deflection, r, at length, x, and concentrated eccentricity, e, between dimensions a and f. Integrally attached to each end is a Compensating Balance Sleeve, comprising a flexible arm with negligible mass, of lengths, L_1 and L_2, spring stiffness's, K_1 and

K_2 and deflections, Y_1 and Y_2, together with equivalent lumped, trim balancing masses, m_1 and m_2, positioned with eccentricities, c_1 and c_2, at their extreme ends. The eccentricity of the lumped masses are positioned 180º out of phase with the shaft eccentricity such that rotation of the shaft produces CFs to act on masses M_s, m_1 and m_2, thereby imparting corresponding deflections r, Y_1 and Y_2, in opposing directions.

Concentrated residual imbalance caused by a localised manufacturing or material defect, or possibly a point of external damage, can be considered as an equivalent additional mass, M_u, acting at radius, R. This is equivalent to a trim balance mass typically fastened to the outer diameter of the shaft, and for the purpose of analysis, is represented by a short zone of length, ($f - a$), with uniform eccentricity, e, and a zone mass, M_p.

Taking mass moments about the axis of rotation and assuming M_u and r are much less than M_p and R, the zone eccentricity approximates to[18]:

$$e \cong \frac{M_u}{M_p}.R \tag{1}$$

Forces Acting on the Compensating Balance Sleeves

According to classical theory[19], the force balance on the compensating balance sleeve can be expressed as:

$$KY = m\omega^2 y \tag{2}$$

From inspection of Figure 1, for small angles of slope, and noting that in the RHS, $(\frac{dr}{dx})_{x=l}$ is negative, the balance mass displacements can be described by:

$$y_1 = Y_1 + c_1 - L_1(\frac{dr}{dx})_{x=0}, \quad \text{and} \quad y_2 = Y_2 + c_2 + L_2(\frac{dr}{dx})_{x=l} \tag{3}$$

$$Y_1 = \frac{-m_1\omega^2\left(L_1(\frac{dr}{dx})_{x=0} - c_1\right)}{K_1 - m_1\omega^2} \quad \text{and} \quad Y_2 = \frac{m_2\omega^2\left(L_2(\frac{dr}{dx})_{x=l} + c_2\right)}{K_2 - m_2\omega^2} \tag{4}$$

with the moments on shaft being:

$$M_{01} = A_{01}\left(\frac{dr}{dx}\right)_{x=0} + B_{01} \quad \text{and} \quad M_{02} = A_{02}\left(\frac{dr}{dx}\right)_{x=l} + B_{02} \tag{5}$$

where $A_{01} = \dfrac{-m_1\omega^2 L_1{}^2 K_1}{K_1 - m_1\omega^2}$ and $A_{02} = \dfrac{m_2\omega^2 L_2{}^2 K_2}{K_2 - m_2\omega^2}$ (6)

$$B_{01} = \frac{m_1\omega^2 c_1 L_1 K_1}{K_1 - m_1\omega^2} \quad \text{and} \quad B_{02} = \frac{m_1\omega^2 c_2 L_2 K_2}{K_2 - m_2\omega^2} \tag{7}$$

The external moment, *Mx*, imposed on the shaft by the balance sleeves at any point *x*, is described by the equation of a straight line between the end moments, M_{01} and M_{02}:

$$Mx = M_{01} + \frac{M_{02} - M_{01}}{\ell}.x \tag{8}$$

From traditional 'Bending of Beams' analysis, the dynamic loading imposed on the shaft is found by differentiating *Mx*, (but noting that $(\frac{dr}{dx})_{x=0}$ and $(\frac{dr}{dx})_{x=l}$ are constant with respect to *x*), giving:

$$\text{Dynamic Loading} = \frac{d^2 Mx}{dx^2} = 0 \tag{9}$$

Forces Acting on the Shaft

At any point, *x,* along the shaft, the eccentricity e_x is given by:

$$e_x = e.[H(x-a) - H(x-f)] \tag{10}$$

where, *H( )*, denotes the Heaviside Function.

Dynamic loading at length *x* on the shaft is obtained by considering the centrifugal force, *CF,* acting on an elemental section δx of shaft:

$$\frac{CF}{\delta x} = \frac{M_s}{\ell}\omega^2(r + e_x) \tag{11}$$

The Combined Assembly

Shaft deflection and reaction loads are determined using standard beam theory analysis of the combined dynamic loading on the shaft resulting from both balancing sleeves and the residual shaft imbalance. Summation of (9) and (11), with (10) substituting for e_x gives:

Total Dynamic Loading =

$$EI\frac{d^4r}{dx^4} = 0 + \frac{M_s}{\ell}\omega^2 r + \frac{M_s}{\ell}\omega^2 e.[H(x-a) - H(x-f)] \tag{12}$$

Constituent parts of (12) are the same as given in [14]; the only differences being the squared brackets containing the Heaviside function, *H*, which limit the eccentricity, *e*, to the shaft portion, *(f - a)*.

The analytical treatment used to solve (12) is omitted for the sake of brevity, and the reader is directed to [14] for details. Specifically, by defining:

$$b^4 = \frac{M_s\omega^2}{\ell EI} \tag{13}$$

the shaft deflection, for any position *x*, is given by:

$$r = R_1 + P.\cos bx - \frac{\frac{M_{02}}{2b^2.E.I} + P.\cos b\ell + \frac{R_{1l}}{2} - \frac{\ddot{R}_{1l}}{2b^2}}{\sin b\ell}.\sin bx + G\cosh bx + H\sinh bx \tag{14}$$

Standard shaft end boundary conditions are applied to this equation to formulate the required parameter definitions and these, together with Heaviside functions and associated parameters are listed in Appendix-2.

Hence, all the parameters required to calculate the shaft deflection from (14), for any position *x*, are now known.

Determining Reaction Loads

To determine the Reaction Loads, from beam theory, the vertical shear force within the beam caused by bending is given by:

$$SFv = EI\frac{d^3r}{dx^3} \tag{15}$$

where at $x = 0$,

$$\left(\frac{d^3r}{dx^3}\right)_{x=0} = (H - \frac{1}{2b}.\left(\frac{dr}{dx}\right)_{x=01})2b^3 \tag{16}$$

and at $x = \ell$,

$$\left(\frac{d^3r}{dx^3}\right)_{x=\ell} = b^3.\left[\frac{\frac{M_{02}}{2b^2.E.I} + P.\cos b\ell + \frac{R_{1l}}{2} - \frac{\ddot{R}_{1l}}{2b^2}}{\sin b\ell}\right].\cos b\ell$$

$$+ \ddot{\ddot{R}}_{1\ell} + Pb^3.\sin b\ell + b^3 G\sinh b\ell + b^3 H\cosh b\ell \tag{17}$$

where:

$$\ddot{\ddot{R}}_{1l} = \left[\frac{eb^3}{2}.\sin b(\ell - a) + \frac{eb^3}{2}.\sinh b(\ell - a)\right].H(\ell - a)$$

$$-\left[\frac{eb^3}{2}.\sin b(\ell - f) + \frac{eb^3}{2}.\sinh b(\ell - f)\right].H(\ell - f) \tag{18}$$

Total reaction force applied to the supports equals internal shear force + external spring force applied by the Compensating Balance Sleeve.

Specifically, at $x = 0$: $\mathrm{Re}_1 = E.I.r_3 + K_1.Y_1$ (19)

and at $x = \ell$, $\mathrm{Re}_2 = -E.I.\ddot{r}_\ell + K_2.Y_2$ (20)

3. Eliminating/Nullifying the Impact of the 1st Critical Speed

From (14) it can be seen that shaft displacement, *r*, becomes infinite, thereby identifying the critical speeds, when $\sin b\ell = 0$, i.e. $b\ell = \pi$, 2π, 3π etc., thereby defining the first critical frequency, from (13), as $\omega_{crit} = (\frac{\pi}{\ell})^2 \sqrt{\frac{\ell.EI}{M}}$. To avoid the singularity, the 3rd term numerator of (14) is also set to zero at $b\ell = \pi$. Therefore, by parameter substitution and equating to zero:

$$-\left(\frac{M_{02}}{2b^2.E.I} + \frac{M_{01}}{2b^2.E.I} + \frac{R_{1l}}{2} - \frac{\ddot{R}_{1l}}{2b^2}\right) = 0 \tag{21}$$

From above definitions, at $b\ell = \pi$,

$$\frac{R_{1l}}{2} - \frac{\ddot{R}_{1l}}{2b^2} = \frac{e}{2}.\left[-\cos ba + \cos bf\right] = e.k$$

Defining the Concentrated Imbalance Coefficient as:

$$k = \frac{\left[-\cos ba + \cos bf\right]}{2} \tag{22}$$

and substitution into (21) gives: $$-\left(\frac{M_{02}}{2b^2.E.I} + \frac{M_{01}}{2b^2.E.I} + e.k\right) = 0$$

Hence, $$M_{01} + M_{02} = -2.k.\left(b^2.E.I.e\right) \tag{23}$$

Equation (23) provides the requirements for balance sleeve compensation to facilitate the elimination/nullification (i.e. move to a higher frequency) of the 1st critical frequency, of a simply supported shaft with concentrated imbalance.

In the case of uniform eccentricity[14], shows that the requirement for "classical" critical speed elimination, (corresponding to $b\ell = \pi$), determines that both balancing sleeve moments are $M_o = b^2.EI.e$. Comparing with the case for concentrated imbalance, this requirement is seen to be a fixed portion of the same equation, since the Concentrated Imbalance Coefficient, *k,* will be a constant for given values of *a* and *f*.

It can also be seen that *k* is an absolute maximum when $a = 0$ and $f = \ell$, giving $k = -1$, i.e. the condition of uniform eccentricity. Under such conditions, from (23):

$M_{01} + M_{02} = 2.b^2.EI.e = 2.Mo$, thereby providing a direct correlation between the analysis for concentrated imbalance and that for uniform eccentricity.

It is notable from (23) that for balancing operations, it is only necessary to estimate the product of the equivalent eccentricity, *e*, and the concentrated imbalance coefficient, *k* (other parameters being known from detail design); this can be regarded simply as an equivalent level of uniform eccentricity and is therefore linearly proportional to the shaft end reaction loads, at any given speed. Hence, it is readily determined from either low speed balancing data or on-site vibration information, and detailed knowledge of individual magnitudes or axial positions of imbalances is not needed.

4. Encastre Simulation

Double encastre mounting (i.e. fixed at both shaft ends) constrains whirling motion of the shaft via the application of fixing moments, M_{f1} and M_{f2} imparted from bearing casings to the ends of the shaft, of sufficient magnitude to maintain shaft-end slopes equal to zero at all operating speeds. The natural frequency then increases by a factor around ~2¼ times that of the equivalent simply supported case (typically). Similarly, single encastre mounting only fixes one end of the shaft with the other remaining simply supported, but in this case the natural frequency is increased by a factor typically of ~1½.

It had previously been shown[14] that a good state of balance is achievable by making the balance sleeve moments as close as possible to the fixing moments, for all operating speeds, but particularly those close to the critical speed. Points of encastre conversion are then produced where exact 'moment equalisation' occurs. It was concluded that the process of critical speed elimination of a simply supported shaft constitutes a conversion process at this speed, to an encastre shaft with a much higher natural frequency. Although this is only theoretically possible due to the critical frequency being irrational, it is apparent that the closer the replication of the balancing moments are to the fixing moments (i.e. the more accurate the encastre approximation), the better the resulting state of balance.

To extend the concept and confirm that these conditions also apply to the more generalised case of a single concentrated imbalance, equivalent double and single encastre shafts have been

analysed. By applying a similar analytical methodology to that previously employed, but with boundary conditions set such that the shaft end slope or bending moment is zero, for appropriate encastre or simply supported cases, the equation for shaft deflection becomes:

$$r = R_1 + P_e.(\cos bx - \cosh bx) + \frac{Q_e}{b}.(\sin bx - \sinh bx) \tag{24}$$

For the double encastre case,

$$P_e = -\frac{R_{1l}.(\cos b\ell - \cosh b\ell) - \frac{\dot{R}_{1l}}{b}.(\sin b\ell - \sinh b\ell)}{2 - 2.\cos b\ell.\cosh b\ell}$$

$$Q_e = -\frac{b.R_{1l}.(\sin b\ell + \sinh b\ell) + \dot{R}_{1l}.(\cos b\ell - \cosh b\ell)}{2 - 2.\cos b\ell.\cosh b\ell}$$

For the single encastre case,

$$P_e = -\frac{R_{1l}.(\sin b\ell + \sinh b\ell) - \frac{\ddot{R}_{1l}}{b^2}.(\sin b\ell - \sinh b\ell)}{2.\sin b\ell.\cosh b\ell - 2.\cos b\ell.\sinh b\ell}$$

$$Q_e = -\frac{b.R_{1l}.(\cos b\ell + \cosh b\ell) + \frac{\ddot{R}_{1l}}{b^2}.(\cos b\ell - \cosh b\ell)}{2.\cos b\ell.\sinh b\ell - 2.\sin b\ell.\cosh b\ell}$$

The double- and single-encastre denominators of P_e and Q_e, become zero and represent the 1st critical speed of the system as $r \to \infty$, when $b\ell = 4.73$ radians and $b\ell = 3.93$ radians, respectively. Compared to results for the simply supported case, the critical speeds are correspondingly 2.27 and 1.56 times higher. Further analysis gives the following fixing moments:

Double encastre:

$$M_{f1} = -2b^2.P_e.E.I \quad \text{and} \quad M_{f2} = E.I.(\ddot{R}_{1l} - b^2.R_{1l} - 2b^2.P_e.\cos b\ell - 2.b.Q_e.\sin b\ell) \tag{25}$$

Single encastre:

$$M_{f1} = -2b^2.P_e.E.I \qquad \text{and} \qquad M_{f2} = 0 \tag{26}$$

Notably, for a speed corresponding to $b\ell = \pi$, the sum of the fixing moment in each case reduces to $M_{f1} + M_{f2} = -e.k.2b^2.E.I$. This is identical to the moment requirement for elimination of the simply supported system, given in (23). Hence, moment equalisation occurs, producing encastre conversion and the critical speed is theoretically eliminated.

The shaft end reaction loads are given by:

$$\mathrm{Re}_1 = -2.Q_e.b^2.E.I \quad \text{and} \quad \mathrm{Re}_2 = -E.I.(\ddot{R}_{1l} + b^3.P_e.[.\sin b\ell - \cosh b\ell] + ... + b^2.Q_e.[-\cos b\ell - \sinh b\ell]) \tag{27}$$

5. Practical Insight

From (23), the sum of the two balancing moments M_{01} and M_{02} determine the condition for critical speed elimination, and the position/length of the concentrated imbalance zone only affects the magnitude of the sum by varying the Concentrated Imbalance Coefficient, *k*, (22).

Hence, near elimination of vibration at the critical speed is achievable using a single compensating balance sleeve fitted at either end. This provides important insight into the characteristics imparted by the compensating sleeve viz. it facilitates increased design flexibility and enables a reduction in the size and cost of components. From a practical perspective, it may still be beneficial to incorporate two balancing sleeves in some instances in order to maintain sensible size and masses, but there remain advantages to be gained from requiring only fine adjustments to be made at one end. This benefits commissioning as access and adjustment time is reduced, especially where applications require a firewall between the prime mover and driven units with separate coupling guard assemblies on either side (which would normally require removal and subsequent re-assembly).

6. Elimination/ Nullifying the Impact of the 2nd Critical Speed

A uniform shaft operating near its 2nd critical speed can be analysed simply as two half-length shafts, connected in series, and operating independently at their 1st critical speeds[20]. Due to symmetry, this is readily confirmed from the earlier assertions that shaft deflection becomes (theoretically) infinite when, $b\ell = \pi$, 2π, 3π etc. thereby defining the critical speeds. Since the 1st critical speed of the half shaft is defined by the condition, $b\ell_1 = \pi$, and the 2nd of the full shaft by: $b\ell_2 = 2\pi$, then $\ell_2 = 2.\ell_1$, i.e. the node point is positioned in the middle of the shaft. However, since it has been shown that the 1st critical speed of the half shaft can be theoretically eliminated by a single compensating sleeve, it similarly follows that the full shaft 2nd critical speed can be eliminated by application of the condition to both half shafts, as shown in Figure 2.

Clearly, each half shaft can be balanced using two compensating sleeves, thereby requiring a 3rd and 4th balancing sleeve either side of the full-shaft node point. At the expense of a small increase in the mass at this point, which is readily trim-balanced since the shaft deflection at this point is zero, theoretical elimination, i.e. practical nullification of the 2nd critical speed, is possible.

For uniform shafts, the analysis can be applied to higher critical speeds due to the symmetry of each section of shaft between the nodes. In most practical circumstances, however, shafts that are not uniform require more complex analysis that is better performed numerically (using FEA for instance). Nevertheless, this simple representation highlights the potential of the proposed system to improve balance for higher order critical speeds.

7. General Imbalance Distribution

Section 2 analysed the case of a single concentrated imbalance. Through superposition the generalised case of any imbalance distribution consisting of a number of concentrated imbalances of varying magnitude, position and angular placement along the shaft, can be analysed by simple vector summation of the individual forces and deflections (under the proviso that the shaft deflections remain small and the material is operating within the linear portion of its stress/strain characteristic). For instance, total reaction loads for a sum of *n* imbalances, in any given plane, is given by:

$$\mathrm{Re}_{(1,2),total} = \sum_{\varphi=1}^{n} \mathrm{Re}_{(1,2),\varphi} \tag{28}$$

Where, φ, is the imbalance index number. This can also be applied to determine the impact of other system variables viz. radial deflection, balance sleeve moment, etc. In addition, individual conditions determined for elimination of critical speeds can also be summed to give the overall condition for elimination of the total imbalance distribution.

8. Equivalent Value of Eccentricity Resulting from Encastre Simulation

Informative insight can be gained by considering the following definition, for shafts without balance correction:

$$Shear\ Force\ Reaction\ Ratio, RR = \frac{S.S.Reaction\ Force}{Encastre\ Reaction\ Force}, \tag{29}$$

This can be determined more readily by considering the special case of uniform eccentricity[14], for simply supported and encastre supported ends.

With reference to Appendix-3, it can be determined that the simply supported, shaft end reaction load is given by:

$$\mathrm{Re}\_ss = \frac{eb^3 EI}{2}.\left(-\frac{1-\cos b\ell}{\sin b\ell} + \frac{1-\cosh b\ell}{\sinh b\ell}\right) \tag{30}$$

And the encastre shaft end reaction load is given by:

$$\mathrm{Re}\_en = -eb^3 EI.\left[\frac{\frac{T+S+\sin b\ell.\sinh b\ell}{T}.(\sin b\ell + \sinh b\ell) - 2.\sinh b\ell}{S}\right] \tag{31}$$

where, $T = 1-\cos b\ell.\cosh b\ell$ and $S = \cos b\ell - \cosh b\ell$

Hence, the Shear Force Reaction Ratio is given by the following equation.

$$RR = \frac{\text{Re}\_ss}{\text{Re}\_en} = \frac{\left(\frac{1-\cosh b\ell}{\sinh b\ell} - \frac{1-\cos b\ell}{\sin b\ell}\right)}{2.\left[\frac{2.\sinh b\ell - \frac{T+S+\sin b\ell.\sinh b\ell}{T}.(\sin b\ell + \sinh b\ell)}{S}\right]} \quad (32)$$

It is notable that eccentricity terms cancel so that the Reaction Ratio is independent of the level of residual eccentricity present in the shaft. Figure 3, shows a plot of Reaction Ratio verses non-dimensional critical speed, from where it can be seen that the ratio greatly increases as the operating speed approaches the critical speed. Since *RR* is inversely proportional to reaction load reduction, and also noting that reaction load is directly proportional to eccentricity, then it follows that this ratio is an indication of the effective, or equivalent, reduction in eccentricity possible under conditions of encastre simulation/maximum compensation.

9. Experimental Verification

To experimentally verify the new theoretical concepts and insight of Balance Sleeve Compensation, a test facility is commissioned comprising of a Bibby Transmissions type TF0027L100 test shaft of 920 mm length tubular spacer (62mm o/d x 56 mm i/d); a disc-type flexible-element coupling-shaft with balance sleeves fitted at each end. The test shaft is mounted between two Oswald, Type QDi13, variable speed, 0 – 20,000 rpm, 49 kW, electric motor/generator units. Figure 4 shows the test facility with the LHS driving and RHS acting as a passive load. The rig is scaled to have the same critical speed as that of a Siemens sub-15MW gas turbine compressor set.

To enable test weights to be mounted on the shaft, and create a-priori identified points of concentrated unbalance, 5x equally spaced dovetail rings are incorporated along the shaft length, as shown in Figures 4 and 5. Tests used two test weights clamped 171° apart, to give a resultant 67.5 g.mm of shaft unbalance, onto the second dovetail ring; thereby providing a length wise, non-symmetric, concentrated point of imbalance.

Detailed construction of the balance sleeves is shown in Figure 5a, where the Balancing Ring corresponds to the theoretical masses, $m_{i,}$ and the combination of Longitudinal Spars provide the lateral bending stiffness' K_i. Detail design determine the structural sizes necessary to meet the parameter requirements given in Table 1 which determined the sleeve's critical speed to be approximately 50% above that of the shaft and also that bending stresses are within practical limits. This process ensured safe operation under the applied imbalances and operating speeds submitted during testing.

Instrumentation consists of 3x Micro-Epsilon, free standing lasers systems (type optoNCDT 2300), positioned to separately enable deflection measurements of i) the LHS sleeve ii) shaft mid-point and, iii) RHS sleeve, as a result of their respective unbalance during shaft rotation. Markers are bonded at the top dead centre (TDC) position on the outside diameter of each laser location to provide a consistent key phaser/trigger point during shaft rotation.

Figure 6 shows a typical laser measurement plot obtained during testing, of cyclic deflection vs time, allowing vector formulation of peak—to–peak deflections and angular offsets between the local heavy spot of section unbalance and the respective laser trigger, i.e. shaft TDC position. Hence, at each test speed it is possible to translate local deflections onto the plane of unbalance produced by the resultant angle of the two test weights, and thereby determine the corresponding components of deflection, amplitude, 0—to–peak, referred to the balance plane. This allows a direct comparison with theoretical results for validation purposes.

Test trials are conducted with designated states of imbalance and compensation, as follows:

i) Residual unbalance only.
ii) Residual unbalance + Test Weight, without Compensation, (Zero Correction).
iii) As ii), with LHS + RHS compensation.
iv) As ii), with mainly LHS compensation.
v) As ii), with solely RHS compensation.
vi) As i), fast transit run through the critical speed.

For comparison purposes, a Mathcad numerical program is employed using parameters given in Table 1, that align with the measured mean value derived from test vi), (two gyroscopic critical speeds, Forward = 10,384 rpm and Backward = 11,093 rpm – not shown).

Theoretical evaluation of the residual unbalance shows that a first order approximation is obtained using a concentrated unbalance of 50% of the test weight, (33.75 g.mm), see Figure 7. Theoretical analysis of the shaft, residual + test weight, then uses a total concentrated unbalance of 150% of the test weight, (101.25 g.mm) for the theoretical comparison shown in Figures 8 - 11.

To provide comparative theoretical mid-point shaft deflections with those of respective test results, the LHS and RHS compensating moments, *Mo1* and *Mo2*, are matched to their respective test measurements of sleeve deflections, at 10,000 rpm, multiplied by the sleeve stiffness and length. A Compensation Ratio consisting of the sum of the measured moments, *Mo1* and *Mo2*, to the theoretically moment requirement for maximum compensation (27.1 Nm) is used to assess the level of compensation present in each test.

Measured moments and the Compensation Ratio for each test trial are given in Table 2.

Figure 8 shows the results of test iii), without compensation and with double sleeve compensation, LHS + RHS, together with their respective theoretical displacements. In this case, with the compensation ratio = 0.654, it is evident that there is a good reduction in shaft deflections, but the shaft is under compensated, and further balance improvements should be possible in this instance.

Figure 9 shows the results of test iv), without compensation and with primarily LHS compensation (but including some residual RHS) together with their respective theoretical displacements. In this case compensation is close to the optimum value (compensation ratio = 1.037) with shaft deflections greatly reduced to only 4% of the non-compensated case.

Figure 10 compares the same test results of Figure 9 with their theoretical equivalent, without compensation, first with standard shaft eccentricity, (concentrated unbalance = 101.25 g.mm) and secondly, with only $1/25^{th}$ of standard eccentricity, (concentrated unbalance = 4.05 g.mm).

Figure 11, shows the results of test v), without compensation and with single sleeve compensation, RHS only, together with their respective theoretical displacements.

It can be seen that this case is under compensated, (compensation ratio = 0.704), and further balance improvements could be made. Nevertheless, it confirms that compensation, or adjustment can be achieved solely by single ended compensation, as predicted by the theoretical analysis.

10. Conclusions

The presented account extends previous, special case, research[14] on compensating balancing sleeves, to demonstrate the suitability of the methodology when applied to a generalized case of a shaft loaded with a single concentrated imbalance. By extension, it is shown that the principle of superposition allows for more practical imbalance distributions to be analysed using vector addition of any number of individual concentrated imbalances, of various magnitude/position. The study shows that the nullification of critical speeds is not dependent on individual discrete values of the balancing moments applied by the balancing sleeves, but on the sum of those moments; the position or size of the imbalance only determining the required magnitude of the sum. Hence, nullification can be achieved by the use of a single compensating balance sleeve fitted at either end of the shaft, thereby replicating a single encastre shaft. It is also shown that the concept can be extended to counter the effects of the 2nd critical speed, and that nullification of higher orders is also possible. This also allows balance corrections to be made at more accessible positions, such as shaft ends, as opposed to inboard positions where higher masses are located; thereby making it useful to those industries where maintenance is difficult or hazardous. The Reaction Ratio, *RR*, is introduced and shown to be independent of any residual shaft eccentricity, indicating that reductions, (additional to any prior balancing procedures), in equivalent levels are possible by a factor of 25, if maximum compensation is achieved. The analysis and insight are supported by test results on a scaled test coupling shaft, as shown in the previous section.

It is apparent that the process of balance sleeve compensation/ encastre simulation has a stiffening effect on a shaft so as to reduce its deflection during operation. Hence, it is envisaged that this process should be beneficial to the majority of flexible shafts, such as those not directly covered by this analysis, but containing discs or other complexity.

It is also notable that for disc applications, where gyroscopic moments both increase and decrease natural frequencies, (with speed), it is only the former, forward whirl modes, that are normally excited by shaft imbalance. In the majority of such cases, the analysis then becomes more conservative, since the critical speed is increased, but the functional characteristics of the balancing mechanism will remain unchanged.

Moreover, since the application of balance sleeve moments could be achieved by a large variety of sleeve designs to suit the individual layout requirements of different machines, it is expected that the benefits afforded by the mechanisms will be used in a wide range of applications sectors.

Acknowledgement

The work presented in this paper is supported by practical case study parameters supplied Siemens Industrial Turbomachinery Limited, Lincoln, United Kingdom.

References

1. Bishop R (1959) The Vibration of Rotating Shafts. *IMechE Part C: J Mechanical Engineering Science* 1: 50-65.

2. Saravanamuttoo HIH. et al (2009) *Gas Turbine Theory*. 6th ed. Harlow: Pearson Education Limited Publishers.

3. API Standard 671, 4th ed. 2007. Special Purpose Couplings for Petroleum, Chemical and Gas Industry Services.

4. Corcoran JP (2003) What is Acceptable Coupling Lateral Critical Speed? *Turbomachinery International* May/ June: 18-21.

5. Thomson WT (1996) *Mechanical Vibrations*. 4th ed. London: Chapman & Hall Publishers.

6. Bishop R. Gladwell G (1959) The vibration and balancing of an unbalanced flexible rotor. *IMechE Part C: J Mechanical Engineering Science* 1: 66-77.

7. Hylton PD (2008) Low Speed Balance for Supercritical Shafting in Gas Turbines. Proceedings of ASME Turbo Expo 2008: Power for Land, Sea and Air, GT2008-50077.

8. Garvey SD et al (2002) Robust balancing for rotating machines. IMechE Part C: J Mechanical Engineering Science 216: 1117-1130.

9. Morton PG (1985) Modal balancing of flexible shafts without trial weights. IMechE Part C: J Mechanical Engineering Science 199: 71-78.

10. Parkinson AG. (1991) Balancing of rotating machinery. IMechE Part C: J Mechanical Engineering Science 205: 53-66.

11. Rodrigues DJ. et al (2006) Automatic balancing of a rigid rotor with misaligned shaft. *Applied Mechanics and Materials* 5-6: 231-236.

12. Burrows CR. Keogh PS. Sahinkaya MN (2009) Progress towards smart rotating machinery through the use of active bearings. *IMechE Part C: J Mechanical Engineering Science* 223: 2849-2859.

13. Rajasekhar M. Srinivas J.Active Vibration Control in Engine Rotors using Electromagnetic Actuation System. *Journal of Mechanical Design and Vibration, 2014, Vol2, No.1, 25-30.*

14. Knowles G et al (2013) Theoretical investigation into balancing high-speed flexible-shafts, by the use of a novel compensating balancing sleeve. IMechE Part C: J Mechanical Engineering Science Article No. 517376.

15. Kirk A, Knowles G et al (2013) Mathematical development and modelling of a counter balance compensating sleeve for the suppression of lateral vibrations in high speed flexible couplings *ASME Turbo Expo* San Antonio, TX, 3-7 June GT2013-95634.

16. ISO 7919-4 2nd Ed 2009-10-01 (2009) Mechanical Vibration – Evaluation of machine vibration by measurements on rotating shafts : Part 4 Gas turbines sets with fluid-film bearings.

17. ISO 10816-4 2nd Ed 2009-10-01 (2009) Mechanical Vibration – Evaluation of machine vibration by measurements on non-rotating shafts : Part 4 Gas turbines sets with fluid-film bearings.

18. Friswell M, Penney J, Garvey S, Lees A (2010) Dynamics of rotating machines. New York Cambridge University Press Publishers.

19. Rhyder GH. (1992) *Strength of Materials*. 3rd ed. Basingstoke: Macmillan Press Publishers.

20. Wilcox JB (1967) *Dynamic Balancing of Rotating Machinery*. London: Pitman Publishers.

Appendix-1

Notation

A_{0i} , B_{0i} , $C_i, D_i, G, H, M, N, P, Q, b$ = Parameters substitutions

BM = Shaft bending moment at point x (Nm)

c_i = Eccentricity of balance sleeve mass (m)

CF = Centrifugal force (N)

e = Eccentricity of concentrated zone (m)

$\hat{e}$ = Euler's number

E = Young's Modulus (N/m^2)

I = 2nd Moment of area in bending (m^4)

K_i = Balance sleeve stiffness (N/m)

ℓ, ℓ_i = Shaft lengths (m)

L_i = Balance sleeve length (m)

m_i = Balance sleeve mass (kg)

M_{0i} = Balance sleeve moment applied at shaft ends (Nm)

M_x = Balance sleeve moment applied to shaft at point x (Nm)

a, f = Eccentric zone end positions (m)

k = Concentrated imbalance coefficient

M_s = Shaft mass (kg)

Mp = Concentrated zone mass (kg)

Mu = Equivalent additional mass (kg)

r = Shaft radial deflection (m)

R_i = Parameters of shaft radial deflection (m)

$\dot{R}_{il}$ = Parameter derivatives of shaft radial deflection

$r_i, \bar{r}, \overline{R_i}$ = Laplace displacement derivatives

R = Radius of rotation of equivalent additional mass Mu (m)

R_{ei} = Reaction load at shaft ends (N)

s = Laplace Transform operator

SFv = Vertical Shear Force

x = Reference point position from shaft end (m)

y_i = Balance mass displacement from rotation axis (m)

Y_i = Balance sleeve deflection (m)

ω = Rotational speed (rad/s)

Appendix-2

Heaviside Functions and intermediary Parameter Definitions:

$$R_1 = \left[-e + \frac{e}{2}.\cos b(x-a) + \frac{e}{2}.\cosh b(x-a)\right].H(x-a) - \left[-e + \frac{e}{2}.\cos b(x-f) + \frac{e}{2}.\cosh b(x-f)\right].H(x-f) \quad \text{(A2.1)}$$

$$R_{1l} = \left[-e + \frac{e}{2}.\cos b(\ell-a) + \frac{e}{2}.\cosh b(\ell-a)\right].H(\ell-a) - \left[-e + \frac{e}{2}.\cos b(\ell-f) + \frac{e}{2}.\cosh b(\ell-f)\right].H(\ell-f) \quad \text{(A2.2)}$$

$$\ddot{R}_{1l} = \left[-\frac{eb^2}{2}.\cos b(\ell-a) + \frac{eb^2}{2}.\cosh b(\ell-a)\right].H(\ell-a) + \left[\frac{eb^2}{2}.\cos b(\ell-f) - \frac{eb^2}{2}.\cosh b(\ell-f)\right].H(\ell-f) \quad \text{(A2.3)}$$

$$C_1 = \frac{B_{02}}{A_{02}} + \dot{R}_{1\ell}, \qquad C_2 = -\frac{b}{\sin b\ell},$$

$$C_3 = -b.\frac{\left(R_{1\ell}. - \frac{\ddot{R}_{1l}}{b^2}\right).\cos b\ell}{2.\sin b\ell}, \qquad C_4 = \frac{b}{\sinh b\ell},$$

$$C_5 = -b.\frac{\left(R_{1\ell}. + \frac{\ddot{R}_{1l}}{b^2}\right).\cosh b\ell}{2.\sinh b\ell}$$

$$C_6 = C_2 + C_4, \qquad C_7 = C_1 + C_3 + C_5 \quad \text{(A2.4)}$$

$$D_1 = -\frac{2b^2.E.I}{A_{01}}, \qquad D_2 = -\frac{B_{01}}{A_{01}},$$

$$D_3 = \frac{1}{2b.E.I.\sinh b\ell} - \frac{1}{2b.E.I.\sin b\ell},$$

$$D_4 = -\frac{b.\cos b\ell}{\sin b\ell}, \qquad D_5 = -b.\frac{\frac{R_{1l}}{2} - \frac{\ddot{R}_{1l}}{2.b^2}}{\sin b\ell},$$

$$D_6 = \frac{b.\cosh b\ell}{\sinh b\ell}, \qquad D_7 = -b.\frac{\frac{R_{1l}}{2} + \frac{\ddot{R}_{1l}}{2.b^2}}{\sinh b\ell},$$

$$D_8 = \frac{D_1 - D_4 - D_6}{D_3}, \qquad D_9 = \frac{D_2 - D_5 - D_7}{D_3} \qquad \text{(A2.5)}$$

$$A_4 = \frac{1}{A_{02}} + \frac{1}{2b.E.I}.\frac{\cos b\ell}{\sin b\ell} - \frac{1}{2b.E.I}.\frac{\cosh b\ell}{\sinh b\ell}$$

$$P = \frac{A_4.D_9 - C_7}{C_6 - A_4.D_8}, \qquad M_{02} = \frac{P.C_6 + C_7}{A_4} \qquad \text{(A2.6)}$$

$$A_1 = -P.2b^2 \quad \text{and} \quad G = -P \qquad \text{(A2.7)}$$

$$H = \frac{\frac{M_{02}}{2.b^2.E.I} - \frac{R_{1l}}{2} - \frac{\ddot{R}_{1l}}{2.b^2} - \frac{A_1}{2b^2}.\cosh b\ell}{\sinh b\ell} \qquad \text{(A2.8)}$$

Appendix-3

The following parameter equations are taken from a previously reported study[14] into cases of simply supported shafts, with uniform eccentricity and balance sleeve compensation.

Shaft end reaction force is the sum of internal shear force and the external spring force applied by the compensating balance sleeve:

$$\text{Re}\_ss = EIr_3 + KY \tag{A3.1}$$

Where, shaft derivatives at $x = 0$ are defined by equations:

$$r_1 = \left(\frac{dr}{dx}\right)_{x=0}, \quad r_2 = \left(\frac{d^2r}{dx^2}\right)_{x=0} \quad \text{and} \quad r_3 = \left(\frac{d^3r}{dx^3}\right)_{x=0} \tag{A3.2}$$

It was further determined that: $r_3 = (H - r_1/2b)2b^3$ (A3.3)

Also, $$H = \frac{\frac{e}{2} + \frac{Mo}{2.b^2.E.I} - (e/2 + A_1/2.b^2).\cosh b\ell}{\sinh b\ell} \tag{A3.4}$$

And $$r_1 = \frac{\frac{eb}{2} - A_3B - \left(eb/2 - A_3B\right)\cos b\ell}{A_4 \sin b\ell} + \frac{\frac{eb}{2} + A_3B - \left(eb/2 + A_3B\right)\cosh b\ell}{A_4 \sinh b\ell} \tag{A3.5}$$

where the following parameters are defined as:

$$A = \frac{-m\omega^2L^2K}{K - m\omega^2}, \quad A_1 = \frac{Ar_1 + B}{EI}, \quad A_3 = \frac{1}{2bEI},$$

$$B = \frac{m\omega^2cLK}{K - m\omega^2}, \quad A_4 = 1 + \frac{A_3A - A_3A\cos b\ell}{\sin b\ell} - \frac{A_3A - A_3A\cosh b\ell}{\sinh b\ell} \tag{A3.6}$$

Also, the balancing sleeve moment is given by: $M_0 = A.\left(\frac{dr}{dx}\right)_{x=0} + B$ (A3.7)

However, for a shaft with zero balance correction, i.e. just a plain shaft with uniform eccentricity, without balance sleeves, then $A,\ A_1,\ B, K, Y$ and M_0 are all zero, giving:

$A_4 = 1$ (A3.8), and by substitution in (A3.4), $H = \dfrac{\frac{e}{2}(1-\cosh b\ell)}{\sinh b\ell}$ (A3.9)

Further from (A3.5): $r_1 = \dfrac{eb}{2}.\left[\dfrac{1-\cos b\ell}{\sin b\ell} + \dfrac{1-\cosh b\ell}{\sinh b\ell}\right]$ (A3.10)

And from (A3.3) $r_3 = \dfrac{eb^3}{2}.\left(-\dfrac{1-\cos b\ell}{\sin b\ell} + \dfrac{1-\cosh b\ell}{\sinh b\ell}\right)$ (A3.11)

The shaft end reaction load consists of internal shear only and from (A3.1) becomes:

$$\text{Re}\_ss = \frac{eb^3 EI}{2}.\left(-\frac{1-\cos b\ell}{\sin b\ell} + \frac{1-\cosh b\ell}{\sinh b\ell}\right) \quad \text{(A3.12)}$$

Similarly analysis of encastre mounted shafts produces the following parameters equations:

$$P_e = \frac{e}{2}.\frac{1+\cos b\ell - \cos b\ell.\cosh b\ell - \cosh b\ell + \sin b\ell.\sinh b\ell}{1-\cos b\ell.\cosh b\ell} \quad \text{(A3.13)}$$

$$J = \frac{P_e(\sin b\ell + \sinh b\ell) - e\sinh b\ell}{\cos b\ell - \cosh b\ell} \quad \text{(A3.14)}$$

Shaft end reaction load is: $\text{Re}\_en = EIr_3$, (A3.15), where, $r_3 = -2.b^3 J$ (A3.16)

Note, in this case the reaction load consists solely of the shaft's internal shear force.

By defining the following parameters: $T = 1-\cos b\ell.\cosh b\ell$ and $S = \cos b\ell - \cosh b\ell$ (A3.17)

and substituting in P_e and again in J, and hence in (A3.16) gives:

$$r_3 = -eb^3.\left[\frac{T+S+\sin b\ell.\sinh b\ell}{T}.(\sin b\ell+\sinh b\ell)-2.\sinh b\ell}{S}\right] \quad \text{(A3.18)}$$

and $$\text{Re}\_en = -eb^3 EI.\left[\frac{T+S+\sin b\ell.\sinh b\ell}{T}.(\sin b\ell+\sinh b\ell)-2.\sinh b\ell}{S}\right] \quad \text{(A3.19)}$$

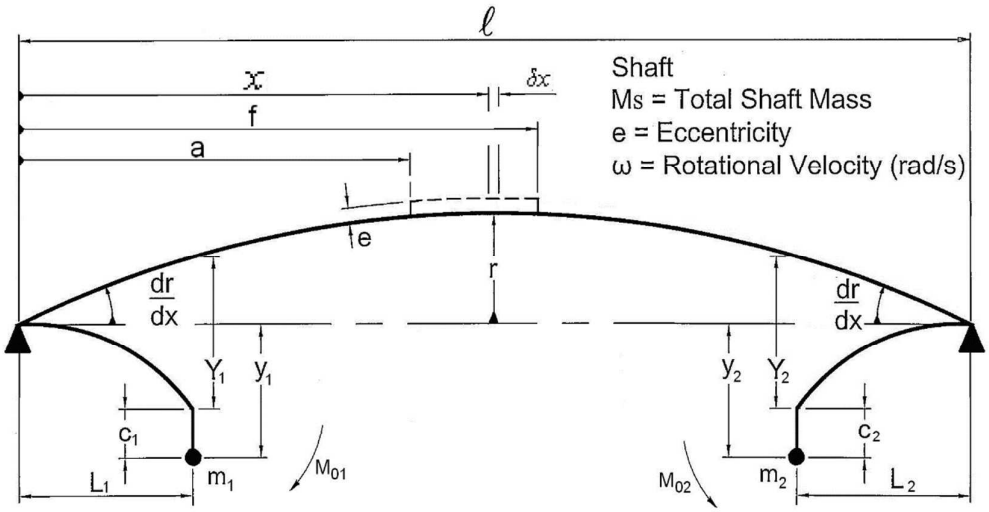

Figure 1, Schematic of simply supported, rotating shaft with concentrated eccentricity

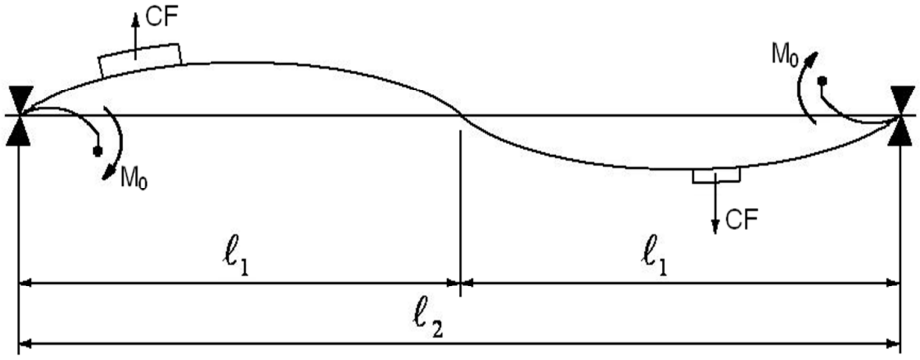

Figure 2, Diagrammatic representation of 2nd critical speed balancing

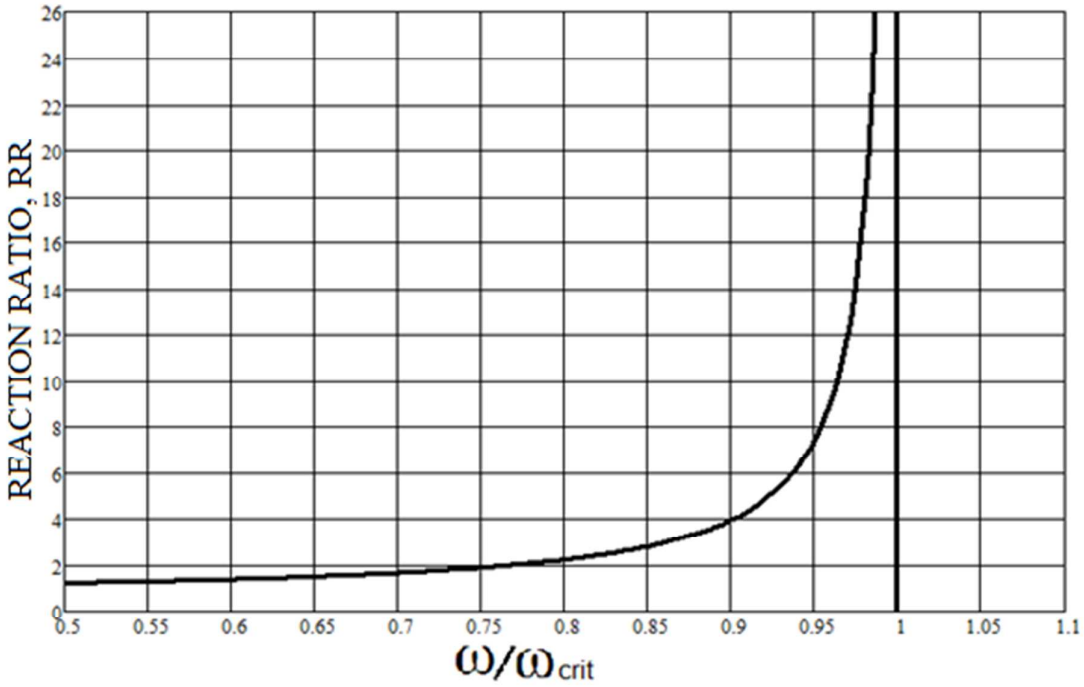

Figure 3, Reaction Ratio, *RR*, verses non-dimensional speed

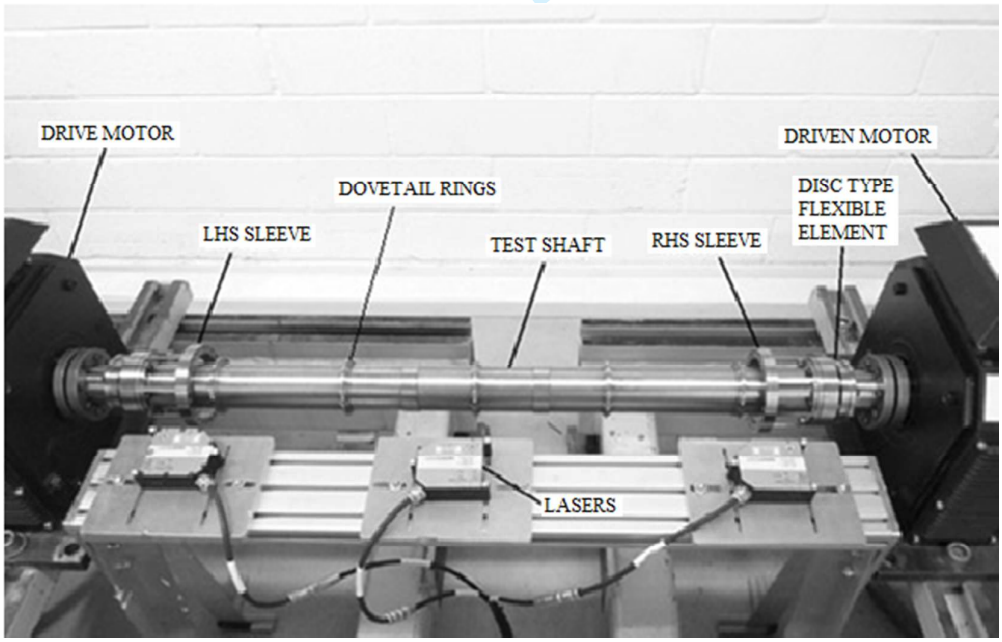

Figure 4, Balance sleeve test facility

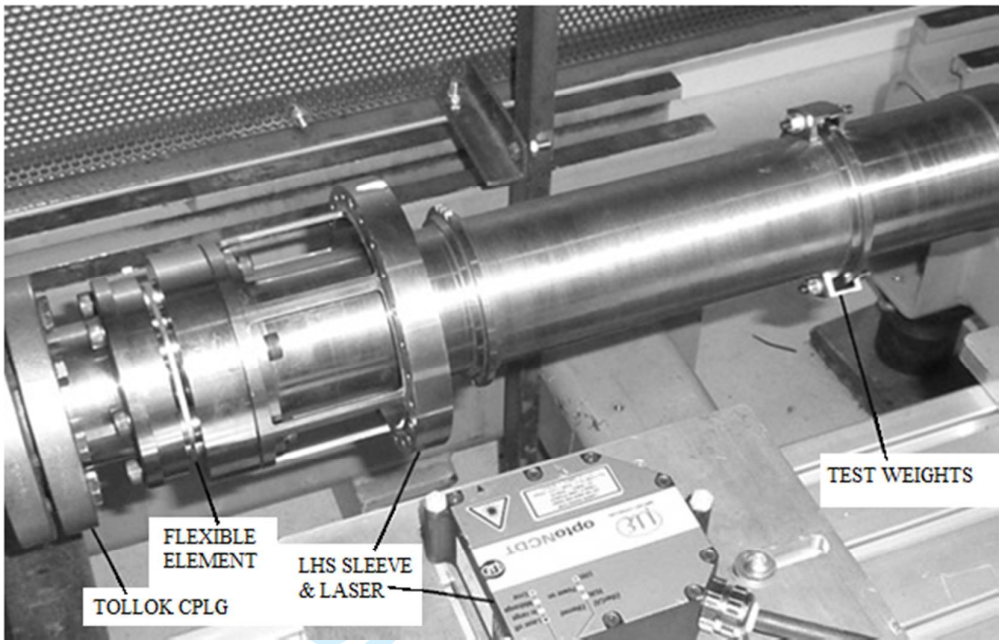

Figure 5, Test weight positions & LHS laser sensing configuration.

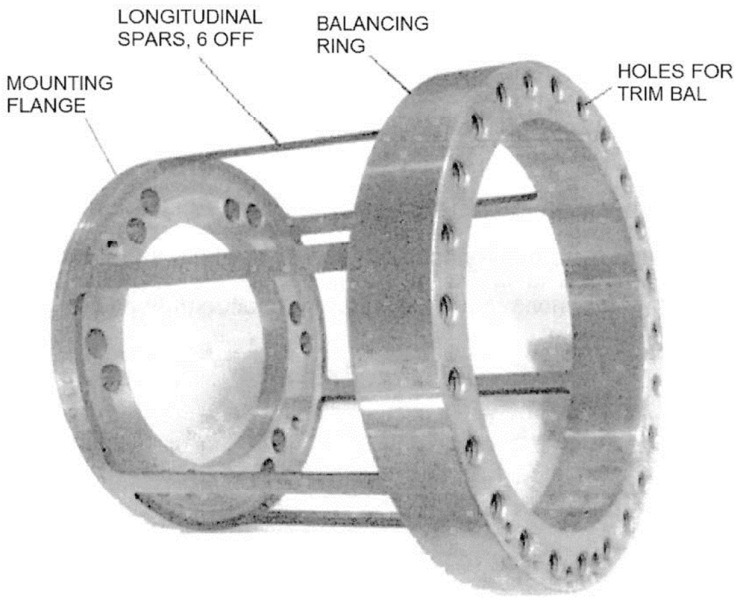

Figure 5a, Balancing Sleeve construction.

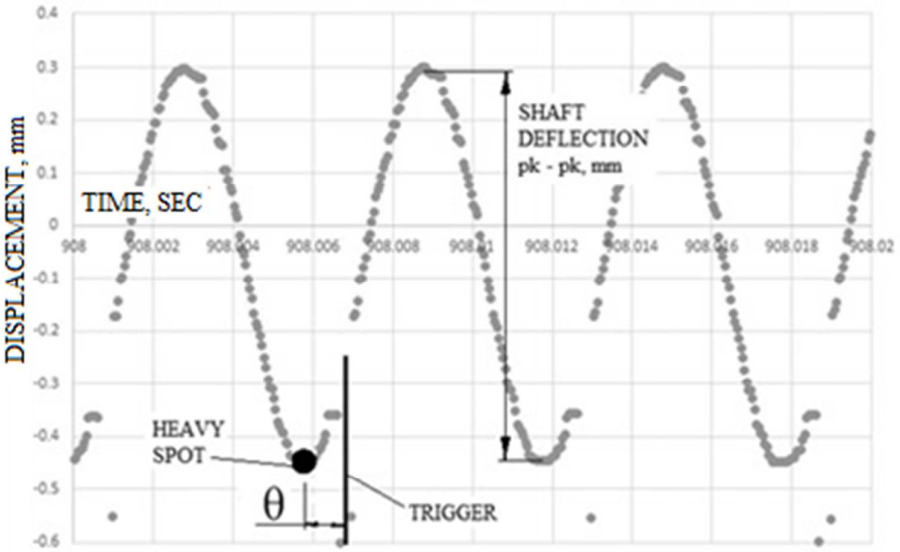

Figure 6, Example laser measurement output.

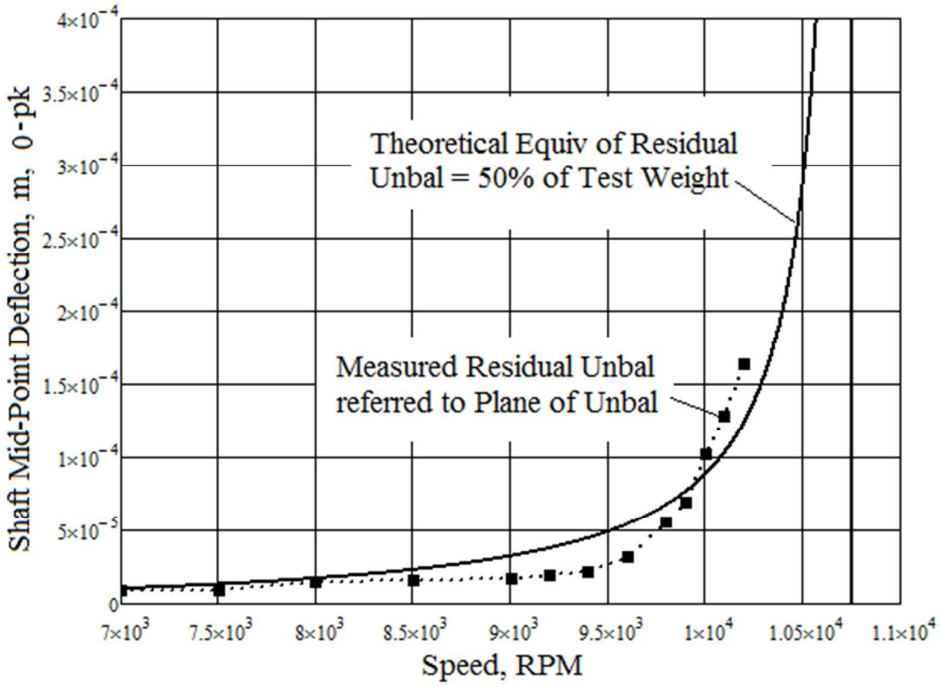

Figure 7, Estimated equivalent theoretical shaft residual unbalance

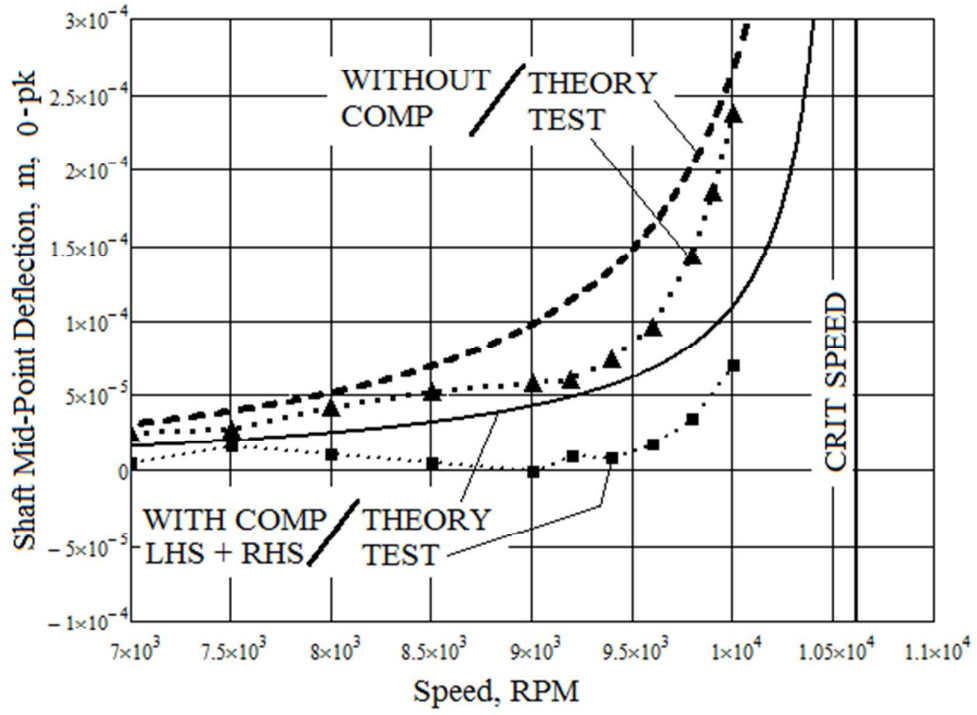

Figure 8, Comparison of Theoretical and Test levels of LHS + RHS Balance Compensation, *CR* = 0.654

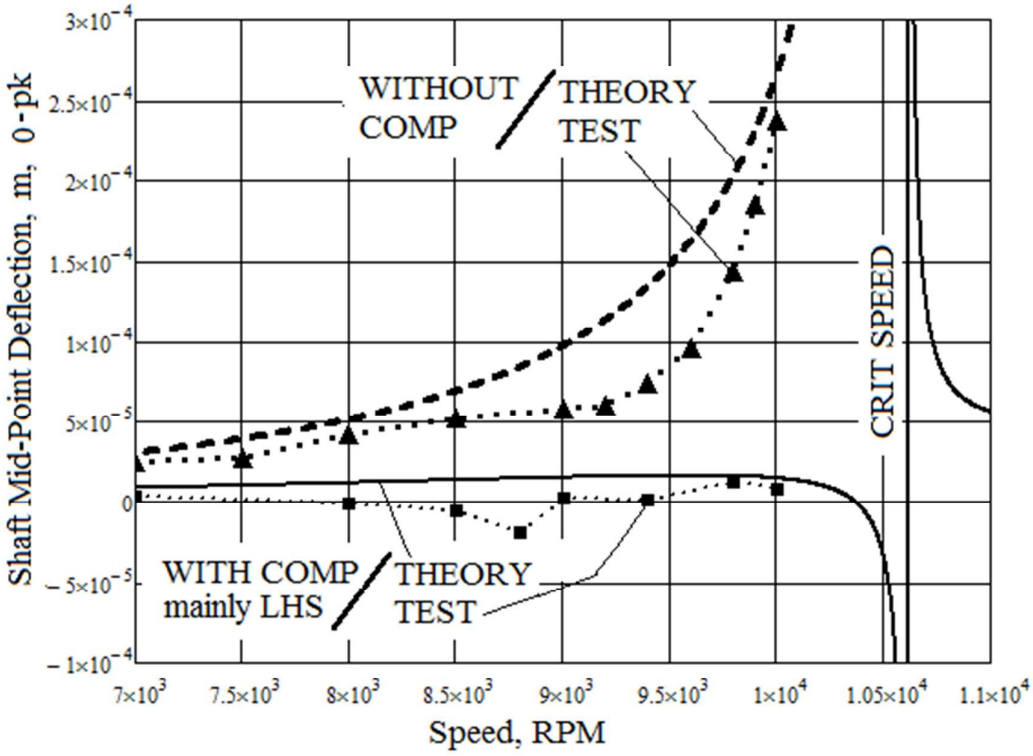

Figure 9, Comparison of Theoretical and Test levels of LHS Balance Compensation, *CR* = 1.037

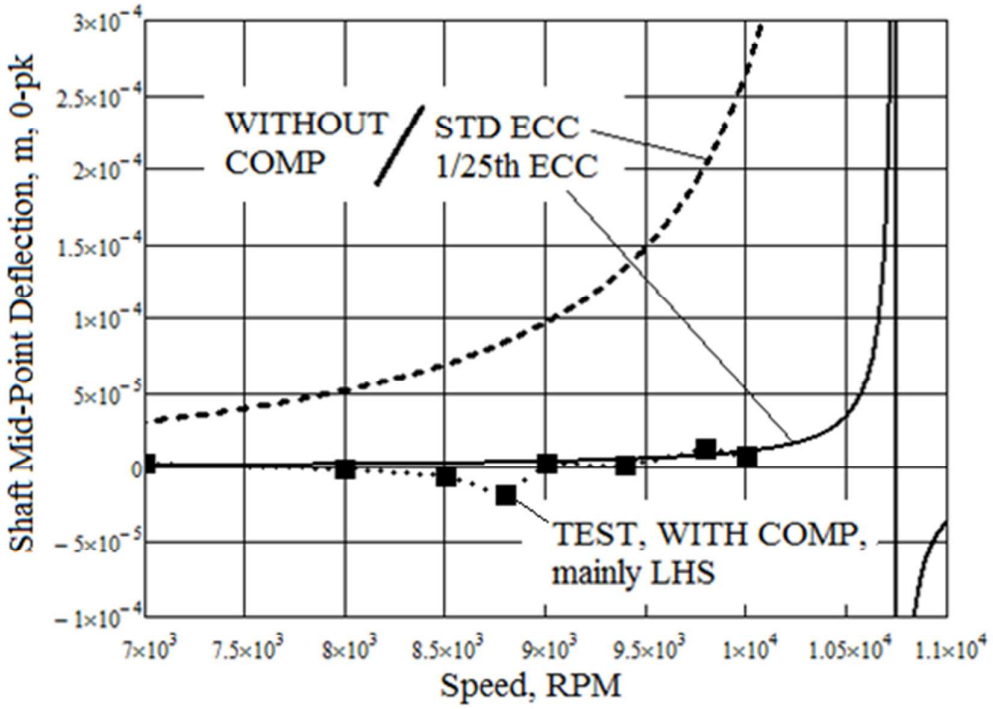

Figure 10, Comparison of Test levels of LHS Balance Compensation, *CR* = 1.037, with theoretical cases of Standard Eccentricity and 1/25th reduced Eccentricity

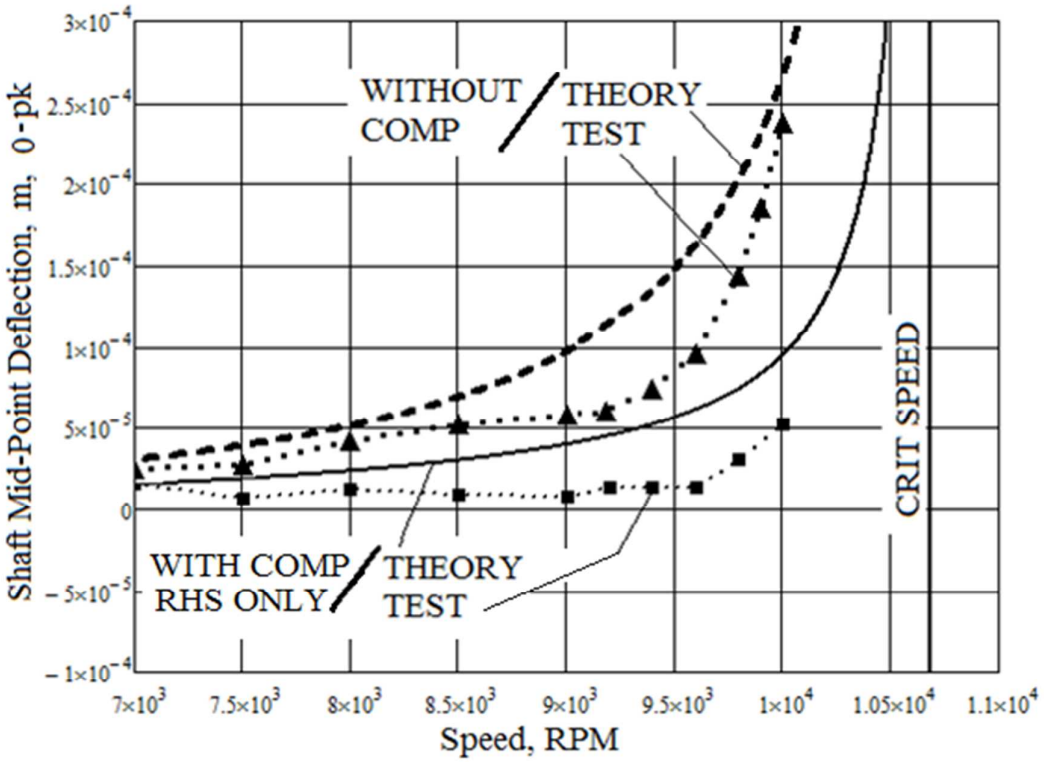

Figure 11, Comparison of Theoretical and Test levels of RHS Balance Compensation, *CR* = 0.710

Test Shaft Parameters	
M_s = 4.2287 kg	ℓ = 0.970 m
m_1 = 0. 3864 kg	m_2 = 0. 3864 kg
e = 0.001549 m	I = 2.426x10^-7 m^4
Figs 8, 9, 10 resp. c_1 = 0.0001119 m c_1 = 0.0004441 m c_1 = 0	Figs 8, 9, 10 resp. c_2 = 0.0003526 m c_2 = 0.0002357 m c_2 = 0.0004774 m
$K_{1,2}$ = 1.136x10^6 N/m	E = 207 x 10^9 N/m^2
$L_{1,2}$ = 0.06148 m	a = 0.318 m
f = 0.328 m	

Table 1, Parameter values used for numerical studies

TEST	MEASURED MOMENTS			COMP RATIO
	Mo1	*Mo2*	Total	
i) Residual unbalance only	0	0	0	0
ii) Residual + Test Weight	0	0	0	0
iii) As ii), with LHS + RHS Comp.	3.74	13.97	17.71	0.654
iv) As ii), with mainly LHS Comp.	18.4	9.7 (residual)	28.1	1.037
v) As ii), with solely RHS Comp.	0	19.07	19.07	0.704
vi) As i), Fast Transit thro' Critical Speed	0	0	0	0

Table 2, Test Details and Compensation Ratio